

Phonon-assisted tunnelling of electrons in a quantum well-quantum dot injection structure

Adam Mielnik-Pyszcorski, Krzysztof Gawarecki and Paweł Machnikowski

Institute of Physics, Wrocław University of Technology, 50-370 Wrocław, Poland

E-mail: Krzysztof.Gawarecki@pwr.wroc.pl

Abstract. We study theoretically phonon-assisted relaxation and tunnelling in a system composed of a quantum dot which is coupled to a quantum well. Within the $\mathbf{k} \cdot \mathbf{p}$ method combined with the Löwdin elimination, we calculate the electron states. We calculate acoustic phonon-assisted relaxation rates between the states in the quantum well and in the quantum dot and study the resulting electron kinetics. We show that transition efficiency crucially depends on the system geometry. We show also that under some conditions, transition efficiency can decrease with the temperature.

PACS numbers: 73.21.La, 73.63.Kv, 63.20.kd

1. Introduction

Quantum dots (QDs) have been proposed for realization of various optical devices. In particular, QD lasers exhibit many advantages such as low threshold current [1, 2, 3, 4], wide spectral tunability [5, 6], or high temperature insensitivity [5, 4, 7, 8, 9, 10]. However, a problem related with the concept of a QD laser is low carrier density inside the dot, which leads to low efficiency [11]. In order to avoid this problem, tunnel injection structures have been developed [12]. Due to high density of states, quantum wells (QWs) are good reservoirs providing carrier supplies for QDs. In a properly designed coupled QW-QD system, carriers can be injected with high speed [11], which considerably increases the optical efficiency. Carrier spectra as well as tunnel coupling have been widely investigated in double quantum dot systems [13, 14, 15, 16, 17, 18]. However, the energy structure in QW-QD system differs significantly from that case, due to the existence of the quasi-continuum of states in the QW. Recently, carrier states in such structures has been calculated within 8 band $\mathbf{k} \cdot \mathbf{p}$ model on a 3D mesh under periodic boundary condition [19].

The carrier kinetics in the QW-QD systems is also strongly affected by phonon-assisted processes which appear in a crystal environment. Carrier-phonon interaction leads to relaxation between states, which can involve carrier transfer (phonon-assisted tunnelling) between the two structures, that is, carrier capture to the QD. The essential role of phonons in the QW-QD injection process is confirmed by experiments [20, 21, 19, 22], which indicate that the magnitude of the relaxation rate highly increases when the energy difference between the states of the QD and the QW becomes comparable with the energy of longitudinal optical (LO) phonons. Theoretically, carrier capture between structures of different dimensionality was studied for various systems and on different levels (Fermi golden rule [23], Boltzmann kinetics [24], Green function formalism [25], and full quantum kinetics [26, 27, 28]) involving LO phonons [23, 29, 24] (also including two-phonon effects [30, 29]) and Coulomb dynamics [24]. The capture process involving tunnelling between a QW and a QD was analyzed within a model including LO phonons and Auger effects, based on a relatively simple model of wave functions [31, 32]. On the other hand, it was shown [33] that the exact shape of wave functions may be important for the correct calculation of the capture rates [33].

In this work, we study theoretically phonon-assisted tunnelling of electrons between a QW and a QD based on the realistic model of wave functions obtained by the $\mathbf{k} \cdot \mathbf{p}$ method for a strained structure. We take into account the electron coupling to acoustic phonons. We show that strain importantly changes the character of the lowest states in the QW (which cannot be accounted for in a simple model). Furthermore, we also investigate the carrier kinetics in the system.

The paper is organized as follows. In Sec. 2, we present the model. In Sec. 3, we discuss the results of the obtained electron states and carrier kinetics. Finally, concluding remarks and discussion are contained in Sec. 4.

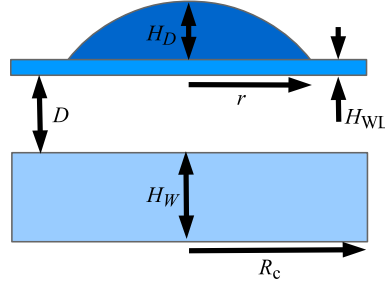


Figure 1. (Color online) The schematic cross-section of the system.

2. Model

We investigate a vertically stacked system composed of a QW and a QD. The schematic picture of the system under consideration is shown in Fig. 1. We assume homogeneous alloying $\text{In}_{0.62}\text{Ga}_{0.38}\text{As}$ inside the dot, $\text{In}_{0.2}\text{Ga}_{0.8}\text{As}$ in the QW and $\text{In}_{0.41}\text{Ga}_{0.59}\text{As}$ in the WL. The QW-layer thickness is set to $H_W = 20$ nm, the WL to $H_{WL} = 0.6$ nm and the QD high to $H_D = 4.5$ nm (see Fig. 1 for the definition of the geometrical parameters). We assume also an axial symmetry of the system and perform the calculations in cylindrical coordinates (ρ, ϕ, z) . Numerical computations are performed in a cylinder with the radius $R_c = 300$ nm and height $H_c = 80$ nm. The results have been verified for convergence with respect to the radius R_c .

The system is strained due to the lattice mismatch between InAs and GaAs. Following our previous work [18], in order to calculate the elements of the strain tensor $\hat{\epsilon}$, we minimized the elastic energy of the system [34, 18] in the continuous elasticity approach. Because of the axial symmetry of the system, the wavefunctions can be represented in the form

$$\psi_n(\rho, z, \phi) = \frac{1}{\sqrt{2\pi}} \varphi_n(\rho, z) e^{iM\phi}, \quad (1)$$

where M is the axial projection of the envelope angular momentum. The local band structure is derived from the 8-band Hamiltonian with strain-induced terms (Bir-Pikus Hamiltonian) using the Löwdin elimination [35, 36]. As a result, we obtain the effective Hamiltonian in the form

$$H_c = -\frac{1}{\rho} \frac{\partial}{\partial \rho} \rho \frac{\hbar^2}{2m_{\perp}(\rho, z)} \frac{\partial}{\partial \rho} - \frac{\partial}{\partial z} \frac{\hbar^2}{2m_z(\rho, z)} \frac{\partial}{\partial z} + \frac{\hbar^2 M^2}{2m_{\perp}(\rho, z) \rho^2} + E_c(\rho, z), \quad (2)$$

with the conduction band edge

$$E_c(\rho, z) = E_{c0} + a_c \text{Tr}\{\hat{\epsilon}\},$$

where E_{c0} is the unstrained bulk conduction band edge. The in-plane component of the effective mass tensor takes the form

$$m_{\perp}^{-1}(\rho, z) = m_0^{-1} \left(A' + \frac{E_P}{2E_{hh}} + \frac{E_P}{6E_{lh}} + \frac{E_P}{3E_{so}} \right)$$

and the z component of the effective mass is

$$m_z^{-1}(\rho, z) = m_0^{-1} \left(A' + \frac{2E_P}{3E_{lh}} + \frac{E_P}{3E_{so}} \right),$$

where

$$A' = \frac{E_p(E_g + 2\Delta/3)}{E_g(E_g + \Delta)},$$

E_P is given by $2m_0P^2/\hbar^2$ (where P is a parameter proportional to the interband matrix transition element), E_g is the energy gap, and energy differences dependent on the position are defined as

$$\begin{aligned} E_{hh} &= E_g + (a_c - a_v)\text{Tr}\{\hat{\epsilon}\} - b_v[\epsilon_{zz} - 0.5(\epsilon_{\rho\rho} + \epsilon_{\phi\phi})], \\ E_{lh} &= E_g + (a_c - a_v)\text{Tr}\{\hat{\epsilon}\} + b_v[\epsilon_{zz} - 0.5(\epsilon_{\rho\rho} + \epsilon_{\phi\phi})], \\ E_{so} &= E_g + (a_c - a_v)\text{Tr}\{\hat{\epsilon}\} + \Delta, \end{aligned}$$

a_c, a_v, b_v are the conduction and valence band deformation potentials. The occupations of the electron states in the QW are given by the Fermi-Dirac distribution with the chemical potential μ , which is related to the surface density of the electrons. For a given chemical potential we calculate the concentration of electrons n_e as a sum over all the occupations in the QW divided by the cylinder base surface (πR_c^2).

The Hamiltonian of the system interacting with acoustic phonons is [37]

$$\begin{aligned} H &= \sum_n \epsilon_n a_n^\dagger a_n + \sum_{\mathbf{k}\lambda} \hbar\omega_{\mathbf{k}\lambda} b_{\mathbf{k}\lambda}^\dagger b_{\mathbf{k}\lambda} \\ &+ \sum_{n,m,\mathbf{k}\lambda} F_{nm\lambda}(\mathbf{k})(b_{\mathbf{k}\lambda} + b_{-\mathbf{k}\lambda}^\dagger) a_n^\dagger a_m, \end{aligned}$$

where ϵ_n denotes the energy of the n -th state, $a_{n\lambda}^\dagger, a_{n\lambda}$ are the creation and annihilation operators for the electron n -th state respectively, $b_{\mathbf{k}\lambda}^\dagger, b_{\mathbf{k}\lambda}$ are operators of creation and annihilation of a phonon with the wave vector \mathbf{k} and phonon branch λ and $F_{nm\lambda}(\mathbf{k}) = F_{nm\lambda}^*(-\mathbf{k})$ is the electron-phonon coupling constant [18]. We find the kinetics of the electrons by solving the Heisenberg equation of motion,

$$\frac{d}{dt} \langle a_i^\dagger a_i \rangle = \frac{i}{\hbar} \langle [H, a_i^\dagger a_i] \rangle,$$

where $\langle a_i^\dagger a_i \rangle \equiv f_i$ is the average occupation of the i -th state.

We perform calculations following the correlation expansion (CE) approach. The detailed derivation is given in the Appendix. As a result, we obtain

$$\begin{aligned} \dot{f}_i &= \sum_{j, \epsilon_j > \epsilon_i} \gamma_{ij} \{f_j(n_B(\omega_{ji}) + 1) - f_i n_B(\omega_{ji}) - f_i f_j\} \\ &+ \sum_{j, \epsilon_j < \epsilon_i} \gamma_{ij} \{f_j n_B(\omega_{ij}) - f_i(n_B(\omega_{ij}) + 1) - f_i f_j\}, \end{aligned} \quad (3)$$

where $\omega_{ij} = (E_i - E_j)/\hbar$ and γ_{ij} is phonon-assisted relaxation rate given by [18]

$$\gamma_{ij} = 2\pi J_{ij}(\omega_{ji}),$$

where $J_{ij}(\omega_{ji})$ is a phonon spectral density,

$$J_{ij}(\omega_{ji}) = \frac{1}{\hbar^2} \sum_{\mathbf{k}\lambda} |F_{ij\lambda}(\mathbf{k})|^2 [\delta(\omega_{ji} - \omega_{\mathbf{k}\lambda}) + \delta(\omega_{ji} + \omega_{\mathbf{k}\lambda})],$$

and n_B is the Bose distribution. Following Ref. [18], we took into account coupling to phonons by deformation potential (DP) as well as piezoelectric field (PE). In order to account how fast charge is flowing into the dot from the QW, we introduce the capture rate as $\gamma_0 = \sum_i \gamma_{0i} f_i (n_B(\omega_{i0}) + 1)$ where we add all relaxation rates from the states in the QW to the ground state (localized in the QD). This procedure describes phonon-assisted relaxation properly if the state in the QD state is completely unoccupied. Otherwise, the Pauli blockade reduces the charge transfer. In consequence, in order to study the time evolution of the occupations, we numerically solve Eq. (3).

The average number of electrons in the QD was found by $\langle N_{qd} \rangle = \sum_i f_i \eta_i$, where η_i is the probability of finding electron in the i -th state in the upper half of the system. The details related with calculations are given in Appendix Appendix A.

3. Results

We calculated single electron states in the considered structure. First, we investigate the influence of strain on electron states. We compared the probability density for the two lowest electron states in a hypothetical structure without strain (Fig. 2(a,b)) and in a real strained structure (Fig. 2(c,d)). In the former case, in order to have similar energy structure as the realistic one, we take a bulk effective mass and we adjust the conduction band edges to fixed values, constant within each structure (QD, QW, barrier). Ground states in both cases are localized in the QD and their character is the same. As shown in the Fig. 2(b), if the strain field is disabled, the probability density of the lowest state in the QW (which has $M = 0$) has a maximum at $\rho = 0$. In the presence of strain (Fig. 2(d)) the character of this state is different and the density forms a ring. This effect is caused by a repulsive potential generated by the strain field from the QD. However, for higher states in the QW (not shown here) this effect vanishes and for the sixth ($M = 0$) state is no longer clearly visible.

Fig. 3 presents the dependence of the two lowest electron energy levels on the distance D . The ground state is (mainly) localized in the dot and the first excited state is localized in the well. For a small distance, there is a strong tunnel coupling which leads to the large splitting between the energy of states in the QD and in the QW.

Next, we investigated the dependence of the capture rate γ_0 on the distance D . The results are shown in Fig. 4(a). The dependence is non-monotonic. On the one hand, for closely spaced structures the wavefunction overlap between the state localized in the QD and those from the QW is large, which is required for an efficient phonon-assisted relaxation process. On the other hand strong coupling leads to the large energy splitting, while the phonon spectral density at high frequencies is low [38, 39]. Therefore, the efficiency of relaxation drops down. At large distances, the wave functions for the initial and final states have very small overlap, hence relaxation is also suppressed.

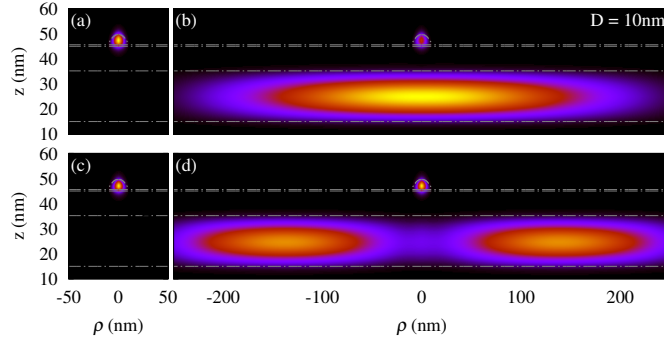


Figure 2. (Color online) The probability density for ground state and first excited state (the lowest state in the QW) in the presence of strain field (a,b) and in the case of neglected strain field (c,d).

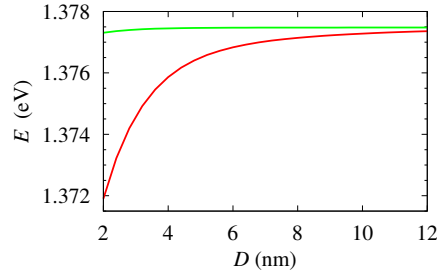


Figure 3. (Color online) The energies of two lowest states in the system as a function of the distance between the dot and the well.

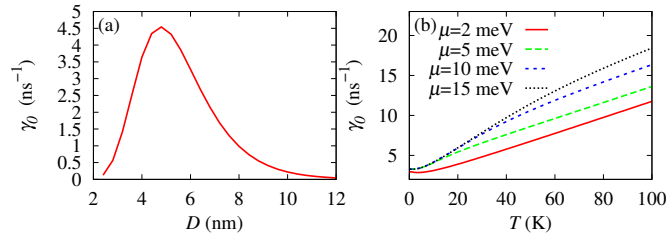


Figure 4. (Color online) (a) The capture rate at $T = 0$ K and $\mu = 15$ meV ($n_e = 1.7 \cdot 10^{11} \text{cm}^{-2}$) as a function of the distance between the dot and the well. (b) Temperature dependence of the phonon-assisted relaxation rate at $D = 4$ nm as a function of the temperature.

We studied also the temperature dependence of the capture rate. In Fig. 4(b) the temperature dependences for several values of the chemical potential (corresponding to $n_e = 2.2 \cdot 10^{10}$ to $n_e = 1.7 \cdot 10^{11} \text{cm}^{-2}$) are shown. Observed dependence is linear at high temperatures because in this case, the leading term of the Bose distribution and Fermi-Dirac distribution is linear ($\sim kT$). The non-zero temperature on the one hand strongly increases the phonon spectral density but also reduces the occupations of electron states below the chemical potential (note that the lowest states in the QW give

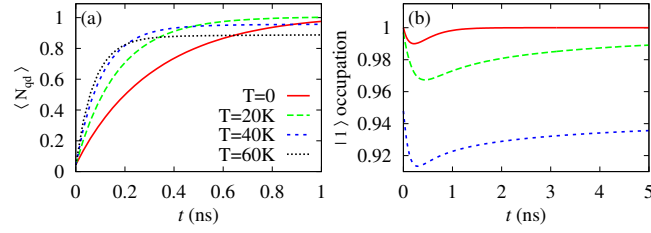


Figure 5. (Color online) (a) The time evolution of the average number of electrons in the QD. (b) The time evolution of the lowest QW state occupation.

the predominant contribution in the relaxation process). The later effect is particularly important at small values of the chemical potential, as shown in Fig. 4(b): for $\mu = 2$ meV ($n_e = 2.2 \cdot 10^{10} \text{ cm}^{-2}$) the relaxation rate decreases with the temperature (for small values of temperature).

We solved Eq. (3) numerically and obtained the electron kinetics. In Fig. 5(a) the time evolution of the average number of electrons in the QD, $\langle N_{qd} \rangle$ is shown. As the initial condition, we assume the zero occupation of the ground state (mainly localized in the dot) and Fermi-Dirac distribution in the well. Because of coupling between the dot and the well, the QW states are also partly localized in the dot and at $t = 0$, the occupation of the QD is about 5 %. During the time evolution electrons from the well tunnel into the dot. The time dependence of N_{qd} is nearly exponential with the initial slope similar to γ_0 (but slightly reduced due to the initial occupation). Increasing the temperature, on the one hand enhances this process, but also enhances the opposite effect (electrons can jump from the dot to the well). At high temperatures the occupation of the dot is reduced because of the thermal redistribution of occupations from the QD to the QW and also due to decreased occupation of the lowest QW states. Fig. 5(b) shows the occupation of the lowest state in the QW. At $T = 0$, the initial occupation is 1, at the beginning of the evolution its value is decreasing because of phonon-assisted tunnelling to the dot. However, this effect is small and does not destroy the exponential character of N_{qd} evolution. However, higher states from the well also relax and full occupation is restored. In the case of non-zero temperature the initial occupation is lowered and electron can be excited to the higher state in the QW. In consequence the initial occupation is no longer recovered.

4. Conclusions

We calculated the electron states in the system of the QD coupled with the QW. We shown that due to the strain-dependent repulsive potential, states in the QW are repelled from the dot axis. We investigated the phonon-assisted tunnelling and relaxation. We obtained non-monotonic dependence of the relaxation rate on the distance between the QW and the QD. We studied the temperature dependence of the phonon transitions and we shown that value of the capture rate can decrease with temperature. Furthermore,

we also investigated the electron kinetics. We obtained the exponential evolution of the average number of electrons in the dot. We also found a nonexponential evolution of the state occupations in the well.

Acknowledgments

This work was supported in parts by the Foundation for Polish Science under the TEAM programme, co-financed by the European Regional Development Fund and by the grant No. 2012/05/N/ST3/03079 from the Polish National Science Centre.

Appendix A. Calculation details

In order to model the evolution of the electron occupations $f_i(t)$ we perform calculation within the CE approach. From the Heisenberg equation for $\langle a_i^\dagger a_j \rangle$ we obtain

$$\begin{aligned} -i\hbar \frac{d}{dt} \langle a_i^\dagger a_j \rangle &= (\epsilon_i - \epsilon_j) \langle a_i^\dagger a_j \rangle \\ &+ \sum_{n, \mathbf{k}\lambda} F_{ni\lambda}(\mathbf{k}) \left(\langle a_n^\dagger a_j b_{\mathbf{k}\lambda} \rangle + \langle a_n^\dagger a_j b_{-\mathbf{k}\lambda}^\dagger \rangle \right) \\ &- \sum_{n, \mathbf{k}\lambda} F_{nj\lambda}^*(\mathbf{k}) \left(\langle a_n^\dagger a_i b_{\mathbf{k}\lambda} \rangle^* + \langle a_n^\dagger a_i b_{-\mathbf{k}\lambda}^\dagger \rangle^* \right). \end{aligned}$$

In a similar way we calculate $\langle a_n^\dagger a_i b_{\mathbf{k}\lambda} \rangle$. Here we assume fast relaxation of the reservoir which allows us to approximate $\langle a_i^\dagger a_j b_{\mathbf{k}'\lambda}^\dagger b_{\mathbf{k}\lambda} \rangle \approx \langle a_i^\dagger a_j \rangle \langle b_{\mathbf{k}'\lambda}^\dagger b_{\mathbf{k}\lambda} \rangle$. Furthermore, we neglected two-phonon processes $\langle b_{\mathbf{k}'\lambda}^\dagger b_{\mathbf{k}\lambda}^\dagger \rangle = \langle b_{\mathbf{k}'\lambda} b_{\mathbf{k}\lambda} \rangle = 0$. After all these simplifications we obtain

$$\begin{aligned} -i\hbar \frac{d}{dt} \langle a_n^\dagger a_j b_{\mathbf{k}\lambda} \rangle &= (\epsilon_n - \epsilon_j - \hbar\omega_{\mathbf{k}}) \langle a_n^\dagger a_j b_{\mathbf{k}\lambda} \rangle \\ &+ \sum_{n'} F_{n'n\lambda}(-\mathbf{k}) \langle a_{n'}^\dagger a_j \rangle n_B(\omega_{\mathbf{k}}) \\ &- \sum_{n'} F_{jn'\lambda}(-\mathbf{k}) \langle a_n^\dagger a_{n'} \rangle (n_B(\omega_{\mathbf{k}}) + 1) \\ &- \sum_{n'm} F_{n'm\lambda}(-\mathbf{k}) \langle a_n^\dagger a_{n'}^\dagger a_j a_m \rangle, \end{aligned}$$

where we took $\langle b_{\mathbf{k}'\lambda}^\dagger b_{\mathbf{k}\lambda} \rangle = n_B(\omega_{\mathbf{k}}) \delta_{\mathbf{k}'\mathbf{k}}$. The electron correlations are accounted for within the Hartree-Fock approximation, $\langle a_i^\dagger a_n^\dagger a_j a_m \rangle \approx \langle a_i^\dagger a_m \rangle \langle a_n^\dagger a_j \rangle - \langle a_i^\dagger a_j \rangle \langle a_n^\dagger a_m \rangle$. This yields a closed set of equations for $\langle a_i^\dagger a_j \rangle$ and $\langle a_i^\dagger a_j b_{\mathbf{k}} \rangle$. The latter is then formally integrated and substituted to the former. Upon performing the Markov and secular approximations, we obtain

$$\begin{aligned} \dot{f}_i &= \sum_{j, \epsilon_j > \epsilon_i} \gamma_{ij} \{ f_j (n_B(\omega_{ji}) + 1) - f_i n_B(\omega_{ji}) - f_i f_j \} \\ &+ \sum_{j, \epsilon_j < \epsilon_i} \gamma_{ij} \{ f_j n_B(\omega_{ji}) - f_i (n_B(\omega_{ji}) + 1) - f_i f_j \}. \end{aligned} \quad (\text{A.1})$$

This set of differential equations is solved numerically using the GSL library [40].

The Schrödinger equation with the Hamiltonian given by Eq. (2) is solved numerically on a two-dimensional grid. The values of material parameters are taken from Ref. [41] except for E_p which was taken 24.0 eV for GaAs and 21.0 eV for InAs. The eigenproblem has been solved using Lanczos method combined with the shift-invert spectral transformation where the linear set of equation is solved using the LIS library [42].

In order to check the validity of modeling an infinite well in a finite cylinder, we calculated the capture rate γ_0 as a function of cylinder radius R_c . We confirmed that γ_0 converge at $R_c = 300$ nm. The reason for this convergence in spite of the quantized spectrum in the cylinder (as opposed to the actual continuum restored in the limit $R_c \rightarrow \infty$) is as follows: when the radius of the cylinder increases, the overlap between the wavefunction in the QD and those localized in the QW decreases like $\sim 1/R_c^2$. On the other hand, with increasing cylinder size, the density of QW states increases as $\sim R_c^2$. As a result, for a sufficiently large cylinder, convergence is reached.

- [1] G. T. Liu, A. Stintz, H. Li, K. Malloy, and L. Lester, *Electron. Lett.* **35**, 1163 (1999).
- [2] M. Asada, Y. Miyamoto, and Y. Suematsu, *IEEE J. Quantum Electron.* **22**, 1915 (1986).
- [3] O. Shchekin and D. Deppe, *IEEE Photon. Technol. Lett.* **14**, 1231 (2002).
- [4] O. Shchekin, J. Ahn, and D. Deppe, *Electron. Lett.* **38**, 712 (2002).
- [5] P. Varangis, H. Li, G. T. Liu, T. Newell, A. Stintz, B. Fuchs, K. Malloy, and L. Lester, *Electron. Lett.* **36**, 1544 (2000).
- [6] D. I. Nikitichev, K. A. Fedorova, Y. Ding, A. Alhazime, A. Able, W. Kaenders, I. Krestnikov, D. Livshits, and E. U. Rafailov, *Appl. Phys. Lett.* **101**, 121107 (2012).
- [7] O. B. Shchekin and D. G. Deppe, *Appl. Phys. Lett.* **80**, 3277 (2002).
- [8] N. Kirstaedter, N. N. Ledentsov, M. Grundmann, D. Bimberg, V. M. Ustinov, S. S. Ruvimov, M. V. Maximov, P. S. Kop'ev, Z. I. Alferov, U. Richter, P. Werner, U. Gösele, and J. Heydenreich, *Electron. Lett.* **30**, 1416 (1994).
- [9] S. Fathpour, Z. Mi, P. Bhattacharya, A. R. Kovsh, S. S. Mikhlin, I. L. Krestnikov, A. V. Kozhukhov, and N. N. Ledentsov, *Appl. Phys. Lett.* **85**, 5164 (2004).
- [10] M. Maksimov, N. Gordeev, S. Zaitsev, P. Kop'ev, I. Kochnev, N. Ledentsov, A. Lunev, S. Ruvimov, A. Sakharov, A. Tsatsul'nikov, Y. Shernyakov, Z. Alferov, and D. Bimberg, *Semiconductors* **31**, 124 (1997).
- [11] P. Bhattacharya, S. Ghosh, S. Pradhan, J. Singh, Z.-K. Wu, J. Urayama, K. Kim, and T. Norris, *IJQE* **39**, 952 (2003).
- [12] Z. Mi, S. Fathpour, and P. Bhattacharya, *Electron. Lett.* **41**, 1282 (2005).
- [13] G. W. Bryant, *Phys. Rev. B* **47**, 1683 (1993).
- [14] M. Bayer, P. Hawrylak, K. Hinzer, S. Fafard, M. Korkusinski, Z. R. Wasilewski, O. Stern, and A. Forchel, *Science* **291**, 451 (2001).
- [15] M. Korkusiński and P. Hawrylak, *Phys. Rev. B* **63**, 195311 (2001).
- [16] A. Schliwa, O. Stier, R. Heitz, M. Grundmann, and D. Bimberg, *Phys. Stat. Sol. (b)* **224**, 405 (2001).
- [17] G. Bester, J. Shumway, and A. Zunger, *Phys. Rev. Lett.* **93**, 047401 (2004).
- [18] K. Gawarecki, M. Pochwała, A. Grodecka-Grad, and P. Machnikowski, *Phys. Rev. B* **81**, 245312 (2010).
- [19] M. Syperek, J. Andrzejewski, W. Rudno-Rudziński, G. Sęk, J. Misiewicz, E. M. Pavelescu, C. Gilfert, and J. P. Reithmaier, *Phys. Rev. B* **85**, 125311 (2012).
- [20] W. Rudno-Rudziński, G. Sęk, K. Ryczko, M. Syperek, J. Misiewicz, E. S. Semenova, A. Lemaitre, and A. Ramdane, *Appl. Phys. Lett.* **94**, 171906 (2009).
- [21] W. Rudno-Rudziński, G. Sęk, K. Ryczko, M. Syperek, J. Misiewicz, E. S. Semenova, A. Lemaitre, and A. Ramdane, *Phys. Stat. Sol. (a)* **206**, 826 (2009).
- [22] G. Sęk, J. Andrzejewski, K. Ryczko, P. Poloczek, J. Misiewicz, E. S. Semenova, A. Lemaitre, G. Patriarche, and A. Ramdane, *Semicond. Sci. Technol.* **24**, 085011 (2009).
- [23] R. Ferreira and G. Bastard, *Appl. Phys. Lett.* **74**, 2818 (1999).
- [24] T. R. Nielsen, P. Gartner, and F. Jahnke, *Phys. Rev. B* **69**, 235314 (2004).
- [25] J. Seebeck, T. R. Nielsen, P. Gartner, and F. Jahnke, *Phys. Rev. B* **71**, 125327 (2005).
- [26] M. Glanemann, V. M. Axt, and T. Kuhn, *Phys. Rev. B* **72**, 045354 (2005).
- [27] D. Reiter, M. Glanemann, V. Axt, and T. Kuhn, *Phys. Rev. B* **73**, 125334 (2006).
- [28] D. Reiter, M. Glanemann, V. Axt, and T. Kuhn, *Phys. Rev. B* **75**, 205327 (2007).
- [29] I. Magnusdottir, A. V. Uskov, S. Bischoff, B. Tromborg, and J. Mørk, *J. Appl. Phys.* **92**, 5982 (2002).
- [30] J.-Z. Zhang and I. Galbraith, *Appl. Phys. Lett.* **89**, 153119 (2006).
- [31] S. L. Chuang and N. Holonyak, *Appl. Phys. Lett.* **80**, 1270 (2002).
- [32] S. W. Chang, S. L. Chuang, and N. Holonyak, *Phys. Rev. B* **70**, 125312 (2004).
- [33] T. Markussen, P. Kristensen, B. Tromborg, T. W. Berg, and J. Mørk, *Phys. Rev. B* **74**, 195342 (2005).
- [34] C. Pryor, J. Kim, L. W. Wang, A. J. Williamson, and A. Zunger, *J. Appl. Phys.* **83**, 2548 (1998).

- [35] T. B. Bahder, Phys. Rev. B **41**, 11992 (1990).
- [36] P. O. Löwdin, J. Chem. Phys. **19**, 1396 (1951).
- [37] A. Grodecka, P. Machnikowski, and J. Förstner, Phys. Rev. B **78**, 085302 (2008).
- [38] K. Gawarecki and P. Machnikowski, Phys. Rev. B **85**, 041305 (2012).
- [39] J. Wu and Z. M. Wang, *Quantum Dot Molecules* (Springer, New York, 2014).
- [40] M. Galassi, J. Davies, J. Theiler, B. Gough, G. Jungman, M. Booth, and F. Rossi, *Gnu Scientific Library: Reference Manual*, 2nd ed. (Network Theory Ltd., <http://www.gnu.org/software/gsl/>, 2003).
- [41] K. Gawarecki, P. Machnikowski, and T. Kuhn, Electron states in a double quantum dot with broken axial symmetry, 2014, arXiv:0706.0858 [cond-mat.mes-hall].
- [42] A. Nishida, *Computational Science and Its Applications - ICCSA 2010*, Vol. 6017 of *Lecture Notes in Computer Science* (Springer, Berlin Heidelberg, 2010), pp. 448–462.